CHARACTERIZATION OF CRACKS AND DELAMINATIONS USING PWAS AD LAMB WAVE BASED TIME-FREQUENCY METHODS

R. Gangadharan, C.R.L. Murthy, S. Gopalakrishnan, M.R. Bhat, D. Roy Mahapatra[1]
Department of Aerospace Engineering
Indian Institute of Science, Bangalore 560012, India
[1]Email: droymahapatra@aero.iisc.ernet.in

Abstract- Use of smart sensor technology along with intelligent signal processing plays a crucial role in the implementation and working of ultrasonic wave based damage detection system. In this work, the interaction of A_0 Lamb mode with damages like crack and delamination are studied. Piezoelectric Wafer Active Sensors (PWAS) are used for generation of Lamb waves to detect damages in metal and composite structures. Experiments were conducted on aluminum plates to study the interaction of Lamb wave with crack oriented at different angles and on a titanium turbine blade of complex geometry with a fine surface crack. A geodesic based Lamb wave approach was employed to locate a crack in an aluminum plate. The existing geodesic algorithm is improved by replacing the Dijkstra's algorithm with the accurate fast marching method. Further, the interactions of A_0 mode with multiple layer delaminations in glass fiber epoxy composite laminates were studied. Spectral Finite Element Method (SFEM) is used for numerical simulation to validate the experimental results. Time-frequency analysis techniques, namely Wavelet Transform (WT) and Hilbert Huang transform (HHT) are used to study the experimental signals and their performances were compared. This study provides significant insight into the problem of identifying localized damages in the structure using integrated PWAS and dispersion of multi-frequency signal after they interact with different types of damage.

Index terms*:* Lamb waves, PWAS, Time-frequency analysis, Composites, Geodesics, Spectral Finite element method, Wavelet transform, Hilbert-Huang transform, Delamination.

I. INTRODUCTION

Ultrasonic wave based Non-Destructive Evaluation (NDE) methods are widely used for interrogating structures to detect the presence of damages of various types, and in recent time, with a greater emphasis towards quantifying these damages. But the conventional NDE methods (e.g., Ultrasonic C-scan, thermography, radiography etc.) require the approximate location of the damage to be known a-priori and that the region being inspected is directly accessible. Further, if the structure is larger and of complex geometry, these NDE methods may not be really suitable for in-situ monitoring of structures. Lamb wave based NDE method is one which has the potential to meet most of these capabilities, that is, (1) large coverage area of inspection due to long distance propagation of Lamb waves (2) no need for direct access of the structure (3) rapid inspection without disassembly (4) adjustable frequency range for interrogation for various size of damage (few millimeter to few centimeter in size). Lamb wave based NDE is most suited for health monitoring of plate and shell type structure with limited extension to thin-walled beams, stiffeners and other parts of airframes.

A damage detection system based on Lamb waves for Structural Health Monitoring (SHM) requires transducers for both excitation and sensing of elastic waves to interrogate the structures in order to detect, locate and characterize defects and damage. The issues of concern in this system are the behavior of the integrated transducers for generation of Lamb waves in the structure, and also the multi-modal and dispersive nature of Lamb waves. While various types of transducers have been explored for this purpose, the advent of piezoelectric active wafer sensors (PWAS) has opened a new direction to SHM applications. PWAS are small, light weight, non invasive and can be embedded inside or mounted on the surface of the structures. Furthermore, they are suitable for Lamb wave actuation and sensing especially for SHM applications of thin-walled structures [1]. Giurgiutiu *et al*. [2] employed PWAS for in-situ SHM of metallic beam and plate structures. A one-dimensional analytical model was derived to predict the electromechanical impedance of the structure measured at the PWAS terminals and was shown that the presence of PWAS embedded in the structure has negligible effect on the electromechanical impedance response. Ihn *et al*. [3] used a piezoelectric actuator/sensor network for detection of fatigue cracks in metallic structures and extended their Short Time Fourier Transform (STFT) technique to the problem of crack growth in riveted structure [4]. Guo *et al.*

[5] studied the interaction of S_0 mode with delaminations in composites and showed that the delamination locations corresponding to the maximum and minimum reflectivities actually correspond to the locations of maximum and minimum shear stresses across the interface under S_0 mode excitation. Hurlebaus *et al*. [6] used a smart PVDF layer for locating the crack and delamination in a composite plate structure. Paget *et al*. [7] embedded PZT discs on composite laminates for damage detection. Su *et al*. [8] presented a comprehensive review on the use of Lamb waves for identification of damage in composite plate type structures.

Damage mechanisms in composites being complicated are difficult to classify and quantify. Numerical modeling of wave propagation in damaged composite structures helps in understanding the wave interaction with damage like reflection, mode conversion etc. It also helps in determining the frequency, duration, shape of the acoustic signal for actuation of bonded/embedded piezo sensors in the structure. Efficient models are required to understand the wave dispersion and scattering in structures. The governing wave equations in the models are usually solved analytically for simple domains and by finite element method or boundary element method for complex domains. But these methods are computationally expensive and time-consuming. Spectral method, in particular the time-Fourier spectral finite element method is often employed for efficient computation. By virtue of its domain transfer formulation using fast Fourier transform and enriched shape function using wavenumber-frequency information, it bypasses the large system size of FEM. The choice of finite element degrees of freedom in this method is governed mostly by the boundary details and the locations of sensors/actuators. The basic framework of Spectral Finite Element Model (SFEM) employed in the present paper can be found in ref. [9] for isotropic solid and in ref. [10, 11] for laminated composite. SFEM is ideally suitable for health monitoring applications such as damage identification and characterization using time history of Lamb wave. This can be used while formulating parameterized model of wave scattering due to crack and delamination type of damages.

Signal processing techniques are essential to analyze sensor signals and extract parametric information regarding damages from often mixed packets of complex Lamb waves. A wide variety of signal processing methods are currently available, namely the time-series analysis, frequency analysis and time-frequency analysis. Time-series methods cannot separate defect scattered composition appropriately from a raw signal containing all parts with various different frequencies. In the frequency domain analysis, we loose the time information, such as arrival

time, wave packet dispersion etc. This problem compels one to combine the time domain information along with the frequency domain information resulting in time-frequency analysis. A time-frequency representation of a signal provides information about how the spectral content of the signal evolves with time, thus providing an ideal tool to analyze and interpret non-stationary signals. This is performed by mapping a one-dimensional signal from the time domain to a two-dimensional time-frequency space. A variety of methods for obtaining the energy density of a function, simultaneously in the time and frequency have been developed, most notably the Short Time Fourier Transform (STFT), Wigner-Ville distribution (WVD), Wavelet Transform (WT) and Hilbert Huang Transform (HHT).

Prosser *et al*. [12] used Wigner-Ville distribution (WVD) to study dispersion of Lamb waves in composite plates. The drawback of WVD compared to other time-frequency representation methods is the presence of cross energy terms, which make time-frequency analysis difficult. The cross terms in WVD is taken care by performing reassignment performance on the smoothed WVD, but the calculations are computationally intensive, difficult to implement and time consuming [13]. Kuttig *et al*. [14] combined chirplet transform with a modified correlation technique to locate the notch in an aluminum plate. Paget *et al.* [7] embedded PZT sensors in composites and conducted experiments to study damages like delamination, impact damage and saw-cut damage. WT was then employed to study the experimental signals and damages were differentiated by looking at the wavelet coefficients. Grabowska *et al*. [15] used WT to study different damages in metallic structure and were able to differentiate fatigue crack from other discontinuities. Benz *et al*. [16] used reassigned spectogram to analyze the interaction of Lamb wave with a notch and proposed correlation technique to locate the notch in an aluminum plate. Ip *et al*. [17] used the Gabor wavelet to extract the dominant wave group from the measured acceleration signals. The wave speed of the fundamental anti-symmetrical Lamb wave mode (A_0) in an aluminum beam was determined and flexural modulus was computed in that work. Pines *et al.* [18] used HHT for health monitoring of civil structures. The signals were studied using HHT and the changes in frequency and magnitude were used to characterize the damage in the structure. It was found that in HHT, serious problems of the spline fitting can occur near the end points, where the cubic spline fitting can have large swings. These end swings can eventually propagate inward during Empirical Mode Decomposition (EMD) and corrupt the whole data, especially in the low frequency band. The problem of end effects in HHT was analyzed and a

method was proposed to remove the end swings in the intrinsic mode functions [19]. Time-frequency analysis of transient dispersive waves was carried out by Apostoloudia *et al.*} [20] and the performances of WVD, WT and HHT were compared by analyzing the flexural waves in beams subjected to an impact load.

The work presented in this paper encompasses extensive experimental investigations to study the interaction of Lamb waves generated using PWAS with different types of discontinuities /defects in metallic as well as composite structures. This included an aluminum plate with crack like defects oriented in different directions, an actual turbine blade made of titanium alloy with a tight surface crack and glass fiber reinforced epoxy composite beam with delaminations in multiple layers. Time-frequency signal processing techniques namely, WT and HHT are applied to the signals obtained experimentally in order to study the dispersive nature of Lamb waves and to extract information about damage present in the structure. The time of flight information from the damage obtained using WT is then used with geodesic algorithm to locate a crack in an aluminum plate. Spectral Finite Element Method (SFEM) is used to model wave propagation in a composite beam structure with delamination. Results obtained from the experiments conducted on glass-epoxy composite beam specimen are validated using the SFEM results. The interaction of A_0 mode with delamination present in multiple layers and the variation of wavelet coefficients of the signal with the number of delamination are studied. In addition, the unwrapped phase variation of the intrinsic mode functions obtained using HHT with delaminations is also studied.

II. TIME-FREQUENCY ANALYSIS

When measured data contain damage events of the structure, it is important to extract the maximum information regarding damage. Time-Frequency representation enables one to understand the signal behavior by creating a frequency estimate at each instant in the signal and thus provides a better understanding of the evolution of the frequencies. In this paper, two techniques namely, the WT and HHT is considered while studying stationary damage and its interaction with dispersive and non-stationary, but linear signals consisting of fundamental A_0 Lamb wave mode.

a. Wavelet Transform (WT)}

In WT, a varying window function is used, which can be dilated and compressed, which is called the mother wavelet. A wavelet is defined using two parameters: a scaling parameter *a*, which is the inverse of frequency and a translation parameter *b*, which translates the window function across the time axis. The continuous wavelet transform of a signal *f(t)* is given by

$$\hat{f}\left(a,b\right)_{WT} = \frac{1}{\sqrt{a}}\int_{-\infty}^{+\infty} f\left(t\right)\psi^{*}\left(\frac{t-b}{a}\right)e^{-j\omega t}dt, \qquad (1)$$

where ψ is the wavelet function. WT overcomes the resolution problem of STFT by letting the resolution of both the time and the frequencies vary in the time-frequency plane in order to obtain a multi-resolution map.

b. Hilbert Huang Transform (HHT)

HHT [19] is suitable for analyzing both nonlinear and nonstationary signals in the time-frequency plane. This method is adaptive, which makes it superior compared to other methods of time-frequency analysis. HHT consists of two parts, one is the Empirical Mode Decomposition (EMD) and the other part is the Hilbert transform (HT). The objective behind EMD is to decompose a measured response signal *x(t)* into intrinsic mode functions (IMF's) that admit well-behaved Hilbert transforms. The instantaneous frequency is obtained by applying HT to each IMF obtained from EMD. The HT of a signal *f(t)* is given by

$$y\left(t\right) = HT\left(f\left(t\right)\right) = \frac{1}{\pi}PV\int_{-\infty}^{+\infty}\frac{f\left(\tau\right)}{t-\tau}d\tau, \qquad (2)$$

in which *PV* indicates the Cauchy principal value of the singular integral. A complex analytic signal *z(t)* is then formed as

$$z\left(t\right) = f\left(t\right) + iy\left(t\right) = a\left(t\right)e^{i\theta\left(t\right)}, \qquad (3)$$

where $i=\sqrt{-1}$, $a\left(t\right)=\sqrt{f^{2}+y^{2}}$ and $\theta\left(t\right)=\tan^{-1}\left(y/f\right)$. Here, *a(t)* is the instantaneous amplitude, θ is the phase function and the instantaneous frequency is $\omega = d\theta/dt$. The limitations in the above steps are that they do not have a proper mathematical basis compared to other time-frequency analysis. Also there are numerical convergence issues in getting the IMF's. Another drawback is the use of spline functions in the EMD, which introduces spurious low frequency oscillations at the beginning and end of the signal time window.

III. SPECTRAL FINITE ELEMENT MODELING OF ELASTIC WAVE PROPAGATION IN COMPOSITE BEAMS

In the present work we are interested in propagation of flexural or A_0 mode in the composite beam structure. The kinematics and field variables chosen for SFEM modeling are based on the A_0 mode only. Substituting the displacement field variables in the governing differential equations for a particular wave propagation problem [10], one obtains the characteristic equation in the frequency-wavenumber (ω, k) space

$$u(x,t) = \sum_{n=1}^{N} \tilde{u}_j e^{-i(k_j x - \omega t)}, \left[\hat{F}(k_j, \omega_n)\right]\{\tilde{u}_j\} = \{0\}, \qquad (4)$$

where *u* is the displacement, $\tilde{u}_j$ is the wave amplitude. This yields a sixth-order characteristic equation in k_j given by

$$Det\left[\hat{F}(k_j, \omega_n)\right] = 0, \quad \forall \omega_n, n = 1, 2, ...N. \qquad (5)$$

Procedure to solve this equation in order to find the wavenumbers $k_j(\omega_n)$ can be found in Refs. (Karunasena *et al.* [24]; Mahapatra and Gopalakrishnan [25]; Gopalakrishnan *et al.*} [26]). In the following sections, we shall use the notation $(\hat{\cdot})$ for Fourier transformed quantitities and $(\tilde{\cdot})$ for its amplitude (wave coefficients).

a. Spectral Finite Element Modeling Approach

In this approach, one is able to utilize the dispersion branches over a suitably broad frequency band. The accuracy of the wavenumber dispersion curves for the problem of Lamb wave propagation in beams and plates depends on the adequate kinematic description of the motion of the material points according to the definition of Lamb wave modes. In most engineering problems, a first-order or third-order shear deformation theory gives sufficiently accurate dispersion curves for the first two Lamb wave modes. After computing the wavenumbers $k_j(\omega_n)$ for a particular sampling frequency ω_n, the displacement vector at a material point is written as

$$\hat{u}(x,z,\omega_n) = \begin{Bmatrix} \hat{u}^0(x,\omega_n) \\ \hat{w}(x,z,\omega_n) \\ \hat{\phi}(x,\omega_n) \end{Bmatrix} = \begin{bmatrix} R_{11} & \dots & R_{16} \\ R_{21} & \dots & R_{26} \\ R_{31} & \dots & R_{36} \end{bmatrix} [\Lambda'] \begin{Bmatrix} \tilde{u}_1 \\ \vdots \\ \tilde{u}_6 \end{Bmatrix} = T'(x,\omega_n)\tilde{u}, \qquad (6)$$

where $\left[\Lambda'\right]$ is a diagonal matrix with exponential entries $\left(e^{-ik_j x}\right)$ [27]. The number of rows in *[R]* corresponds to in-plane displacement, transverse displacement and first-order rotation. The number of column in *[R]* depends on the completeness of the wave modes. These wave modes are independent and hence they are automatically obtained by solving the singular value problem in Eqn. (4) in the polynomial eigen value framework. Here, the first two are for in-plane wave in positive and negative x-direction and the rest of the four are two propagating components of flexural-shear wave and two attenuating components. The type of attenuation and direction of propagation depend on the real and imaginary parts of k_j and its sign. By evaluating Eqn. 6 at the element nodes at *x=0, L* (for one-dimensional element) the element nodal displacement vector can be expressed as

$$\hat{u}^e = \begin{bmatrix} T'\left(x,\omega_n\right)_{x=0} \\ T'\left(x,\omega_n\right)_{x=L} \end{bmatrix} \tilde{u} = T''\tilde{u}. \quad (7)$$

The non-singular complex matrix T'' represents the local wave characteristics of the displacement field. Eliminating the unknown wave coefficient amplitude vector $\tilde{u}$ from Eqn. (6) using Eqn. (7), the generic displacement field $\hat{u}\left(x,\omega_n\right)$ can be expressed in terms of the nodal displacements as

$$\hat{u}\left(x,\omega_n\right) = T'\left(x,\omega_n\right)T''^{-1}\hat{u}^e = \bar{N}\left(x,\omega_n\right)^e \hat{u}^e, \quad (8)$$

where $\bar{N}\left(x,\omega_n\right)$ is the exact/enriched spectral element interpolation function matrix. Next, the natural boundary conditions are evaluated for *x=0, L* which yield the element nodal force vector $\hat{f}^e$ as

$$\hat{f}^e\left(\omega_n\right) = \begin{bmatrix} -Q'R\Lambda'_{x=0} - Q''R\Lambda''_{x=0} \\ -Q'R\Lambda'_{x=L} + Q''R\Lambda''_{x=L} \end{bmatrix} T''^{-1}\hat{u}^e\left(\omega_n\right) = \hat{K}^e\left(\omega_n\right)\hat{u}^e\left(\omega_n\right), \quad (9)$$

where $\hat{K}^e\left(\omega_n\right)$ is the spectral finite element stiffness matrix and it is a complex matrix function of frequency unlike the form $-\omega^2 M + K$ as obtained via *hp*-FEM with polynomial space interpolation. Q' and Q'' are both real matrices whose entries are the functions of the cross-sectional stiffness. Λ'' is a diagonal matrix obtained as

$$\Lambda''_{jj} = \frac{\partial}{\partial x}\Lambda'_{jj}. \quad (10)$$

For those kinematic descriptions of material points in the plane of wave propagation (e.g., higher order beam, plate and layered system) where the complete wave vector is to be considered instead of a scalar wavenumber as in case of simple beam, it is not always possible to construct an exact spectral element. However, it is possible to construct an enriched spectral element for a given *h-p* refinement using incomplete set of dispersion curves (k,ω) [28]. In the next section we discuss the SFEM for modeling Lamb wave interaction with delamination.

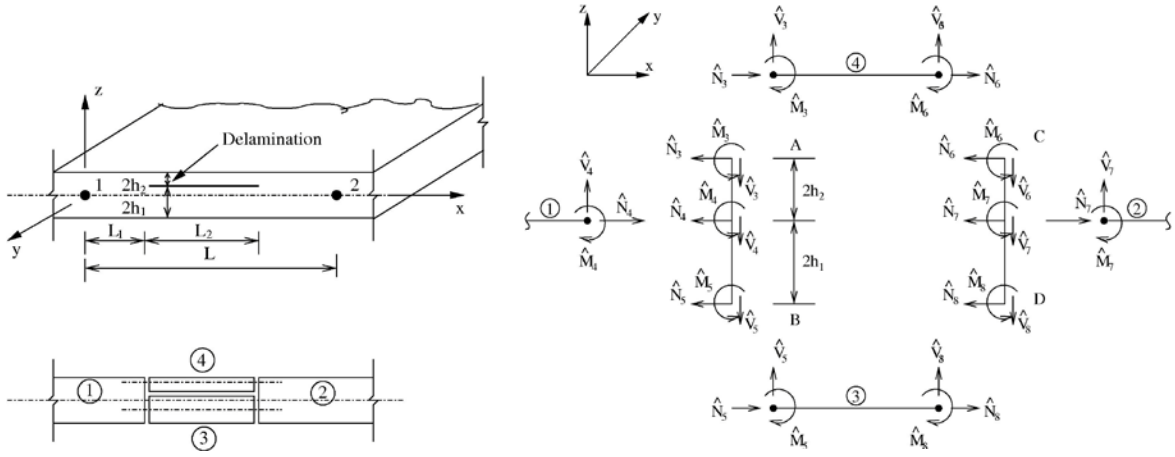

(a) (b)

Figure 1. (a) Modeling of an embedded delamination with base-laminates and sub-laminates (1D waveguide). Waveguide 1-2: base-laminates; Waveguide 3-4: sub-laminates. (b) Force balance at the interface between base-laminate and sub-laminate elements

IV. MODELING OF WAVE PROPAGATION THROUGH DELAMINATED BEAMS

The location of the nodes of the spectral elements for a delaminated beam is shown in Fig. 1a. In the absence of delamination, a single spectral element between node-1 and node-2 is sufficient. This is of great advantage that a very small system of equations is to be solved at each frequency while adopting a suitable parameter estimation scheme like neural network, genetic algorithm (see [27, 29, 30]) etc. The presence of delamination, when treated as structural discontinuity by neglecting the effect of stress singularity at the delamination tip, increases the number of elements from one to four. Six more nodes are introduced to model individual base-laminates and sub-laminates. For the sub-laminate-elements (element-3 and 4), the nodes are located at the mid-plane of the sub-laminates, and element lengths are equal to the length of the delamination. The

kinematic assumption for the interface of base-laminate and sub-laminates is that the cross-section remains straight, that is, the slope is continuous and constant at the interface. Under this assumption, one obtains the following kinematic relationship between the nodal degrees of freedom:

$$\hat{u}_3 = \begin{Bmatrix} \hat{u}_3^0 \\ \hat{w}_3 \\ \hat{\phi}_3 \end{Bmatrix} = \begin{Bmatrix} \hat{u}_4^0 + h_2\hat{\phi}_4 \\ \hat{w}_4 \\ \hat{\phi}_4 \end{Bmatrix} = \begin{bmatrix} 1 & 0 & h_2 \\ 0 & 1 & 0 \\ 0 & 0 & 1 \end{bmatrix} \begin{Bmatrix} \hat{u}_4^0 \\ \hat{w}_4 \\ \hat{\phi}_4 \end{Bmatrix} = S'\hat{u}_{4,} \quad (11)$$

$$\hat{u}_5 = \begin{Bmatrix} \hat{u}_5^0 \\ \hat{w}_5 \\ \hat{\phi}_5 \end{Bmatrix} = \begin{Bmatrix} \hat{u}_4^0 - h_2\hat{\phi}_4 \\ \hat{w}_4 \\ \hat{\phi}_4 \end{Bmatrix} = \begin{bmatrix} 1 & 0 & -h_2 \\ 0 & 1 & 0 \\ 0 & 0 & 1 \end{bmatrix} \begin{Bmatrix} \hat{u}_4^0 \\ \hat{w}_4 \\ \hat{\phi}_4 \end{Bmatrix} = S''\hat{u}_4 \quad (12)$$

for the left interface of the delamination, and similarly,

$$\hat{u}_6 = S'\hat{u}_7,\ \hat{u}_8 = S''\hat{u}_7 \quad (13)$$

for the right interface of the delamination (see Fig. 1).

For the equilibrium of forces at the left interface *AB* (Fig. 1b), one can derive the following force balance equation in frequency domain as

$$\begin{Bmatrix} \hat{N}_4(\omega_n) \\ \hat{V}_4(\omega_n) \\ \hat{M}_4(\omega_n) \end{Bmatrix} + \begin{Bmatrix} \hat{N}_3(\omega_n) \\ \hat{V}_3(\omega_n) \\ \hat{M}_3(\omega_n) \end{Bmatrix} + \begin{Bmatrix} 0 \\ 0 \\ h_2\hat{N}_3(\omega_n) \end{Bmatrix} + \begin{Bmatrix} \hat{N}_5(\omega_n) \\ \hat{V}_5(\omega_n) \\ \hat{M}_5(\omega_n) \end{Bmatrix} + \begin{Bmatrix} 0 \\ 0 \\ -h_1\hat{N}_5(\omega_n) \end{Bmatrix} = \begin{Bmatrix} 0 \\ 0 \\ 0 \end{Bmatrix}, \quad (14)$$

where $\hat{N}, \hat{V}, \hat{M}$ stand for frequency domain axial force, shear force and bending moment, respectively. Equation (14) can be rewritten in matrix form as

$$\hat{f}_4 + S'^T \hat{f}_3 + S''^T \hat{f}_5 = 0. \quad (15)$$

Similarly, from the equilibrium of the right interface *CD*, one has

$$\hat{f}_7 + S'^T \hat{f}_6 + S''^T \hat{f}_8 = 0. \quad (16)$$

After a finite element assembly of Eqns. (9), (15) and (16), one has the global system equation:

$$\begin{bmatrix} \hat{K}_{11}^{(1)} & \hat{K}_{12}^{(1)} & 0 & 0 \\ \hat{K}_{21}^{(1)} & \begin{pmatrix} \hat{K}_{22}^{(1)} + S'^T \hat{K}_{11}^{(4)} S' \\ + S''^T \hat{K}_{11}^{(3)} S'' \end{pmatrix} & \left(S'^T \hat{K}_{12}^{(4)} S' + S''^T \hat{K}_{12}^{(3)} S'' \right) & 0 \\ 0 & \left(S'^T \hat{K}_{21}^{(4)} S' + S''^T \hat{K}_{21}^{(3)} S'' \right) & \begin{pmatrix} \hat{K}_{11}^{(2)} + S'^T \hat{K}_{22}^{(4)} S' \\ + S''^T \hat{K}_{22}^{(3)} S'' \end{pmatrix} & \hat{K}_{12}^{(2)} \\ 0 & 0 & \hat{K}_{21}^{(2)} & \hat{K}_{22}^{(2)} \end{bmatrix} \times \begin{Bmatrix} \hat{u}_1 \\ \hat{u}_4 \\ \hat{u}_7 \\ \hat{u}_2 \end{Bmatrix} = \begin{Bmatrix} \hat{f}_1 \\ 0 \\ 0 \\ \hat{f}_2 \end{Bmatrix}. \quad (17)$$

Performing stationary condensation at each sampling frequency (ω_n) for the degrees of freedom at the internal nodes-4 and 7, the final form of the equilibrium equation for the delaminated beam is obtained as

$$\hat{\bar{K}}(\omega_n) \begin{Bmatrix} \hat{u}_1(\omega_n) \\ \hat{u}_2(\omega_n) \end{Bmatrix} = \begin{Bmatrix} \hat{f}_1(\omega_n) \\ \hat{f}_2(\omega_n) \end{Bmatrix}, \quad (18)$$

where $\hat{\bar{K}}$ is the effective dynamic stiffness matrix for the *spectral element with embedded delamination*. Now, one only needs to replace an usual spectral element with this {\it spectral element} with embedded delamination wherever a possible delamination may exist, keeping the original FE mesh unaltered. The parameters hidden inside are (h_1, h_2, L_1, L_2), see Fig. 1. Hence, it is evident that insertion of this parameterized element with a modular approach is very much suitable for faster modeling and simulation.

V. EXPERIMENTAL DETAILS

The experimental setup consists of a NI-PXI 6115 DAQ card, preamplifier and voltage amplifier. The schematic of the experimental setup is shown in Fig. 2. Using analog output of the NI-DAQ card, a tone burst signal was generated. This signal was further amplified using a voltage amplifier and applied to the PWAS transmitter for generation of Lamb waves in the structure. The low energy waves picked up by the PWAS receiver was amplified by the inbuilt low noise high frequency preamplifier. The NI-DAQ card was used to collect the signal from the pre-amplifier and signal was stored in the computer for further signal processing. The Labview software was used to filter the unwanted noise from the signal. The PWAS sensors (APC 850) used were 10mm in diameter and 1mm in thickness.

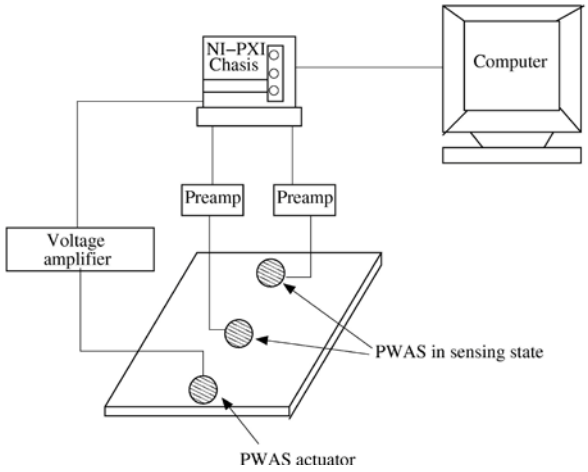

Figure 2. Schematic diagram of the experimental setup

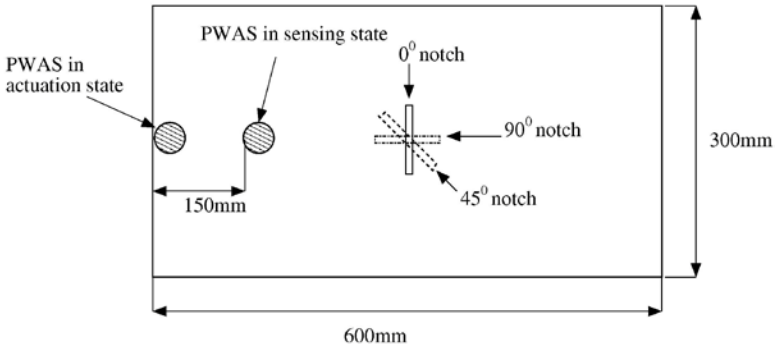

Figure 3. Schematic diagram of the aluminum plate with various different notch configurations.

a. Aluminum plate with crack

Experiments were carried out on an aluminum plate of dimensions *600mm x 300mm x 3mm*. The PWAS sensor was bonded at a distance of 150mm from the actuator (Fig. 3). The group velocity of A_0 mode is obtained experimentally and is in close agreement to the theoretical values as shown in Fig. 4. Damages in the aluminum plates were introduced by machining 0^o, 45^o and 90^o through thickness crack of dimensions 50mm length and 3mm width at a distance of 300mm from the left end of the structure. The A_0 Lamb wave mode acquired by the sensor for various angle cracks is shown in Fig. 5. A similar numerical study with different crack orientations was carried out by Kogl *et al*. [31] and they used the higher harmonics of the excitation frequency introduced by the nonlinearity of the defect to locate the crack. WT is applied and the continuous wavelet transform of the signals are shown in Fig. 6. The contour plot of the wavelet coefficients indicates clearly the location of defect and also by looking at their magnitude the orientation of

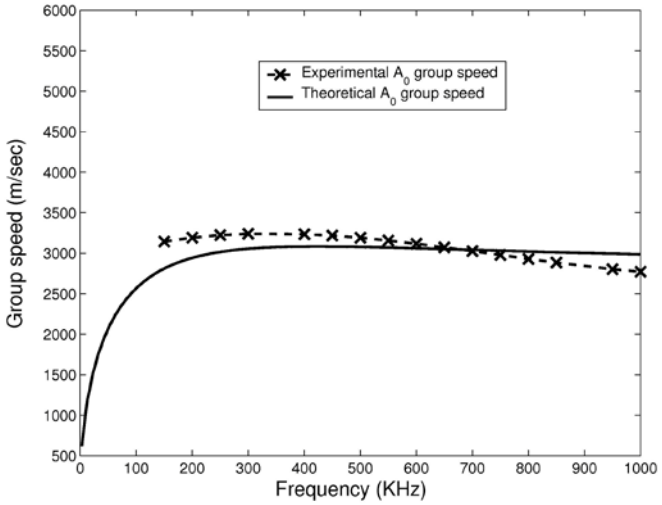

Figure 4. Dispersion curve for aluminum - experimental and theoretical A_0 mode group velocity.

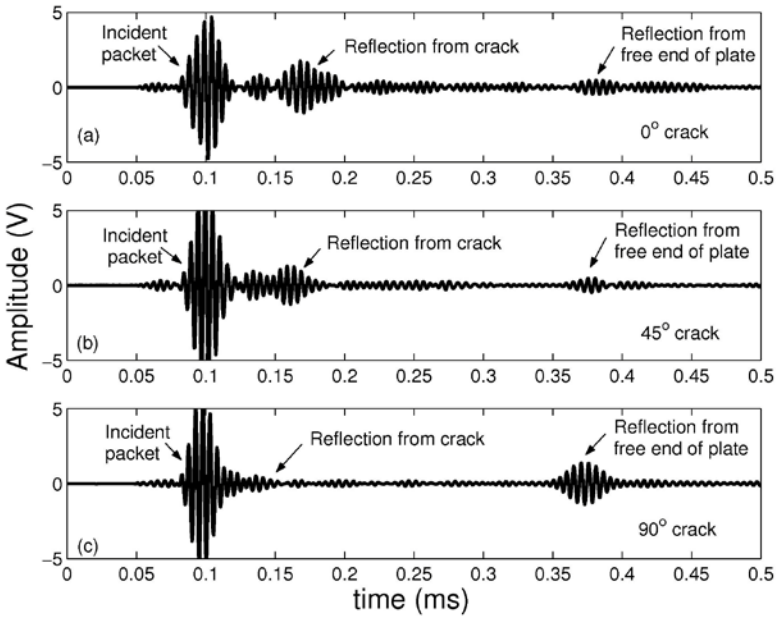

Figure 5. Experimental study of wave propagation in aluminum plates with different crack orientation.

the defect in the plate structure can be correlated. The wavelet coefficients of the signals are computed at 200KHz and is shown in Fig. 7. The amplitude of the wavelet coefficients of the reflected wave from defect is high for 0^o, 45^o orientation of crack and less for 90^o crack. In the case of 0^o, 45^o crack configurations, the interaction of waves with crack results in decrease in the magnitude of wavelet coefficients of the reflected wave packet from the free boundary of the plate. For 90^o crack the high magnitude value of the wavelet coefficient of the reflected wave from the free boundary of the plate indicates that more energy is transferred across the crack as

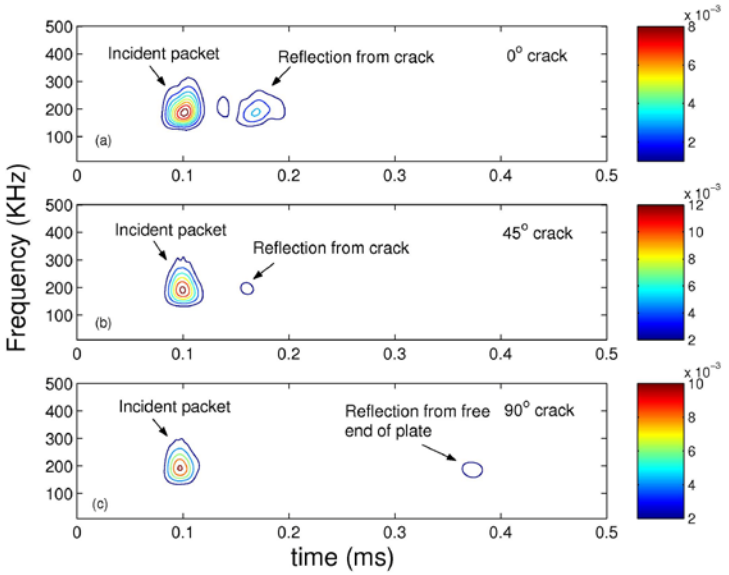

Figure 6. Time-frequency map obtained from sensor signal for Aluminum plate with different crack configurations: Contour shows the continuous wavelet transform coefficients of the signals.

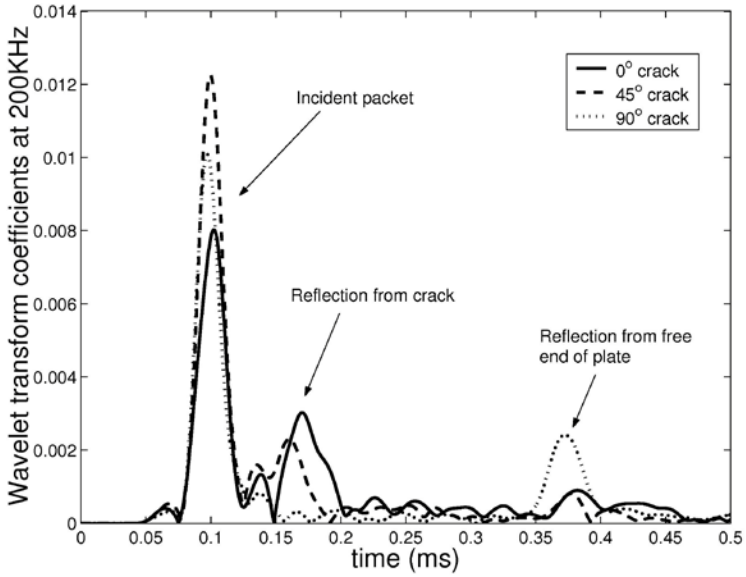

Figure 7. Aluminum plate with various different crack configurations: Wavelet transform coefficients of the signal at 200 KHz.

there is less interaction of waves with notch. The HHT is then applied to the acquired signals shown in Fig. 5 and the first intrinsic mode function (IMF) is shown in Fig. 8. The first IMF captures the highest frequency components present in the signal and removes the unwanted lower frequency components. In this case, the highest frequency is close to 200KHz from the higher side of the narrow bandpass filter used. The instantaneous phase is computed only for the first

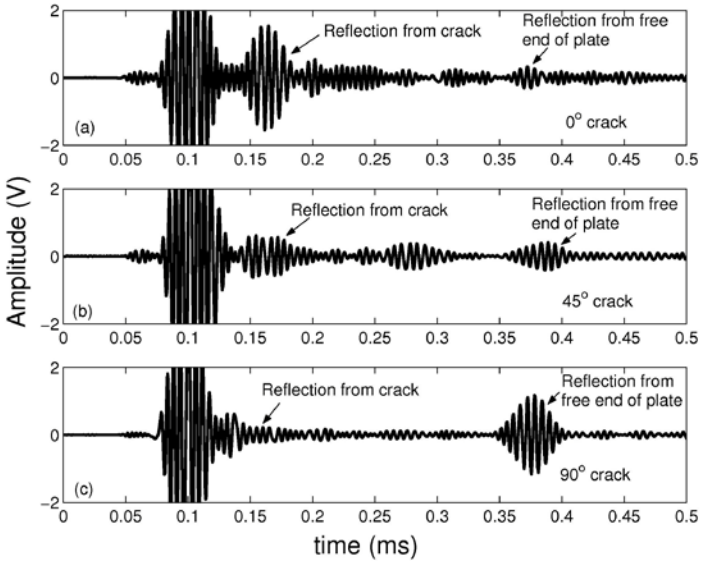

Figure 8. First Intrinsic Mode Function (IMF) of the sensor signal for Aluminum plate with various different crack configurations.

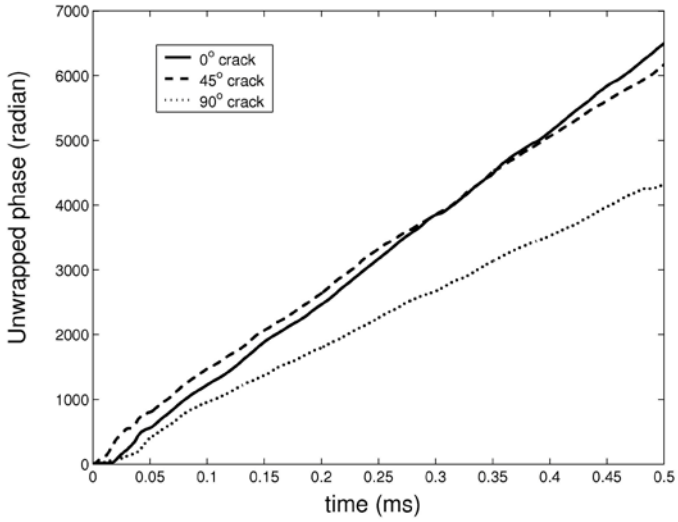

Figure 9. Evolution of unwrapped phase of sensor signal obtained by HHT for various crack orientations.

IMF and the phase information is used as a damage detection tool. Unwrapped phase is then computed in order to obtain a monotonically increasing phase function with time. The local change in slope of the unwrapped phase is related to the presence of damage in the structure. The unwrapped phase of the IMF1 for each crack configuration is computed and is shown in Fig. 9. The unwrapped phase also indicates the number of oscillations of the wave and the increase in slope of unwrapped phase variation for 0^o and 45^o is attributed to the presence of more reflection

of waves from the crack. In the case of 90^o crack, the reflection of waves from notch is very small and the slope of unwrapped phase variation is below the other crack configurations. From this plot, we can conclude that the reflection from the damage is interpreted by a slope change in the Hilbert phase and the slope change appears to be dependent on the size and orientation of the crack as seen in the Fig. 9. Thus, the Hilbert phase allows the size and orientation of damage to be determined. These results give us an insight regarding the interaction of the A^0 mode with crack of different orientations.

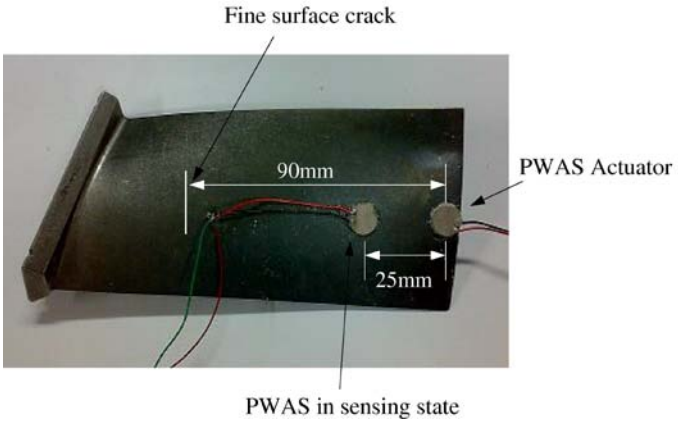

Figure 10. A gas turbine blade made of Titanium with a poorly visible fatigue crack at the surface.

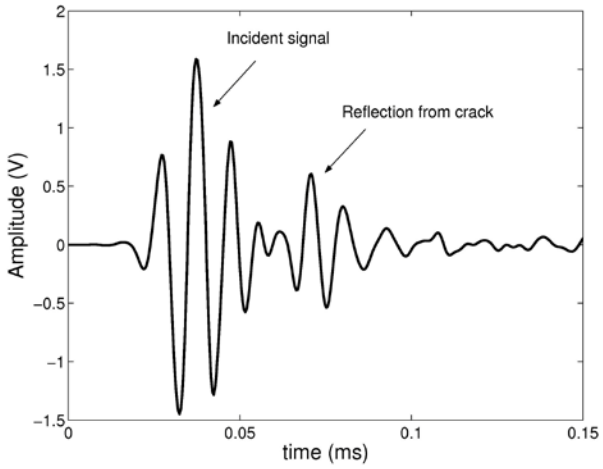

Figure 11. Signal picked up by sensor in titanium blade with crack.

b. Detection of small surface cracks in Gas turbine blades

Experiments were carried out on a gas turbine blade made of titanium with a complex geometry as shown in Fig. 10. The damage in the form of surface crack was induced by fatigue loading. In order to suppress the reflection from the edges of the blade, modeling clay was applied on the

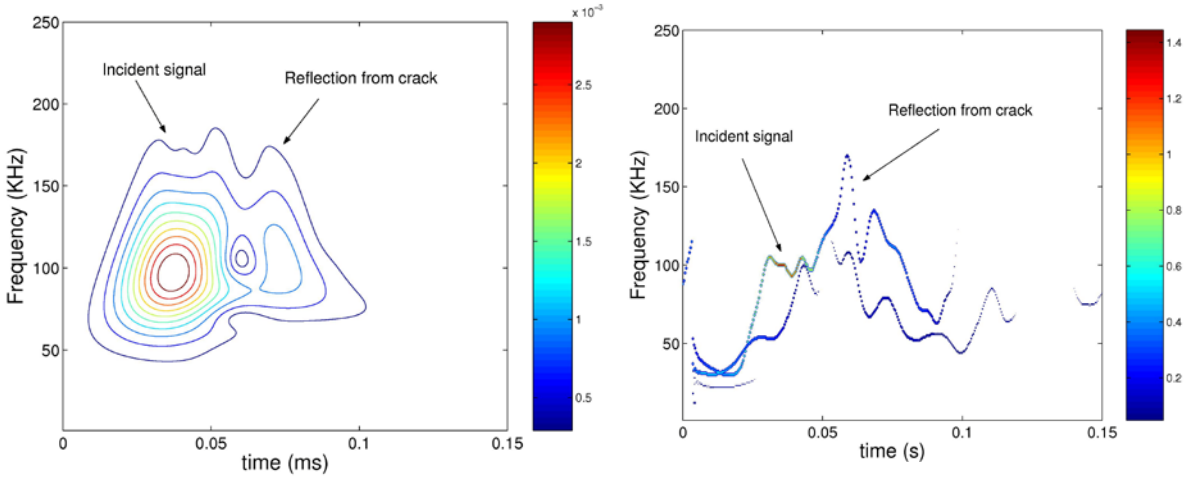

(a) (b)

Figure 12. Time-frequency map obtained from sensor in the titanium blade with crack (a) Continuous wavelet transform (b) Hilbert Huang transform. Color bar indicates the magnitude of the WT or HHT coefficient

edges to absorb the unwanted reflections. The PWAS for actuation was bonded at the right end of the blade to excite the Lamb wave mode in the structure. A Hanning window toneburst signal of 4 cycles centered at 100KHz was applied to the PWAS. The generated wave picked up by the sensor at 25mm from the actuator is shown in Fig. 11. The continuous wavelet transform and the Hilbert energy density of the signal is shown in Fig. 12a and 12b, respectively. The contour map of both WT and HHT clearly indicates the reflection from the crack in the time-frequency plane. The group speed of the A_0 mode is determined experimentally to be 2000m/s from the time of flight information. Using the group speed value of Lamb wave mode, the location of the crack is found out to be 86.5mm from the actuator. The location of the crack position was then determined using eddy current testing method and the crack was located at 90mm from the actuator position. The eddy current and Lamb wave results are close to each other and the difference in the crack location can be attributed to the assumption of constant group velocity in turbine geometry with varying thickness and curvature along the length of the blade.

The results in this section show that Lamb waves along with time-frequency analysis methods can be used for extracting damage information's like defect orientation and time of flight information. In the next section, a geodesic based Lamb wave approach using the time of flight information from damage is employed to identify the damage location in a metallic plate structure.

VI. LOCATION OF A CRACK IN AN ALUMINUM PLATE USING GEODESIC METHOD

The geodesic approach proposed by the authors [32] has been used in this work to locate the defect in the structure. In the present work the geodesic algorithm is improved by replacing the simpler Dijkstra's algorithm with fast marching method (FMM) to compute accurately the discrete geodesics in the discretized structure. The drawback of Dijkstra's algorithm is the geodesic path was restricted to the triangle edges, and sometimes it can lead to incorrect results. In fast marching method the geodesic path can pass through the triangular faces of the mesh and, thus the shortest path obtained between two points in a triangular mesh using FMM is more accurate than Dijkstra's algorithm. The geodesic algorithm involves a two step strategy of first computing the discrete geodesics numerically using FMM followed by locating the damage through the intersection of these geodesics from the sensor array based on voronoi diagram concept.

a. Geodesic formulation

Let t_1, t_2 be the time taken by the wave generated from the damage *S* to reach the sensors *S1, S2* respectively. The difference in time for the wave reaching the two sensors given by $dt = t_1 - t_2$ is proportional to distance difference between the source and the sensors. Hence, the governing equation is given by,

$$D(S1-S) - D(S2-S) = Vdt. \qquad (19)$$

where *V* is the velocity of the wave in the structure. The only unknowns in the Eqn. 19 are the locations of the damage. Hence by forming enough distance-time-difference equations we can solve for the damage location. This can be seen as an implicit function,

$$\Phi(D, V, dt) = 0. \qquad (20)$$

The above Eqn. 20 combines the information from geometry of the surface (geodesics) and the information from the material (velocity), with the experimental observation (*dt*). The geodesics $\{D\}$ in above formulation are computed numerically on the triangular mesh using FMM.

b. Fast marching method (FMM)

Fast marching method is a numerical algorithm introduced by Sethian [33] to study the motion of propagating interfaces. FMM on triangulated surfaces was proposed by Sethian and Kimmel [34] to compute the shortest path between two points in the mesh. The general idea for FMM was borrowed from the graph theory and is a direct extension of Dijkstra's algorithm. FMM computes for each point x on the mesh the time of arrival $T(x)$ of the wave front originating from the source node x_0. The initial approximation of $T(x)$ is, like in Dijkstra's algorithm, zero at x_0 and infinity elsewhere. The algorithm classifies the points of the mesh into three categories (Fig. 13). Black points are points where the arrival time has been computed and since the wave front is assumed to propagate only in forward direction these values are not going to change in the future. Gray points are unprocessed points, for which the arrival time has not been computed yet. White points are those belonging to the propagating wave front, which can be considered an interface between the black and the gray regions of the mesh. Initially, only the source x_0 is marked as black and all points adjacent to it are marked as white. The remaining points are marked as gray. Like Dijkstra's algorithm, at each iteration we process the white point with the smallest value of $T(x)$ by updating the approximation of all the non-black points in triangles sharing it. The white point is then tagged as black and the updated adjacent points are tagged as white. The process continues until all points become black. In geodesic algorithm, FMM is used to compute the shortest path accurately from the sensor nodes to other nodes in the mesh.

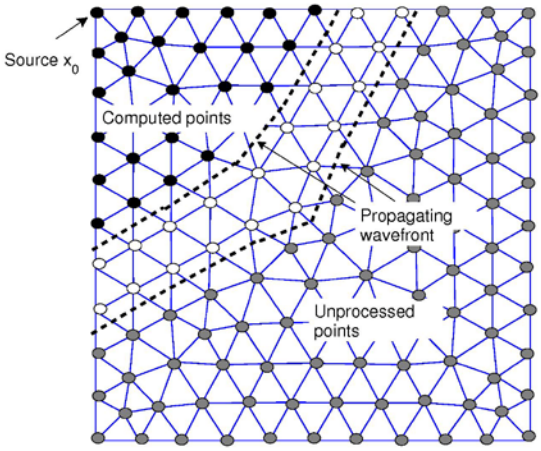

Figure 13. Fast marching method algorithm..

c. Voronoi diagram concept

The second part of the algorithm is the construction of voronoi like diagram to locate the damage using the intersection of geodesics from the sensors. The implementation of Voronoi diagram concept is explained below. For a given mesh,

1) Let *nk* be the k^{th} node in the mesh,

2) *D(nkSi)* be the distance between k^{th} node and i^{th} sensor and,

3) $Dk\left(S_{ij}\right)$ be the difference in distances of a node *k* from sensors *Si* and *Sj*,

i.e., $Dk\left(S_{ij}\right) = D\left(nkSi\right) - D\left(nkSj\right)$.

4) Voronoi line between any two sensors *Si* and *Sj* is formed by nodes which satisfy the condition that $Dk\left(S_{ij}\right) = Vdt_{ij}$ where, dt_{ij} is the hit arrival-time difference between the sensor *Si* and *Sj* and *D's* are geodesic distances and the corresponding line can be seen as set of these nodes which is given by

$$L_{ij} = \left\{ nk \mid Dk\left(S_{ij}\right) = Vdt_{ij} \right\}. \quad (21)$$

5) The intersection point or damage location in the set L_{ij} is given by

$$S = \left\{ n \mid \left(L_{12} \cap L_{23} \cap L_{13} \right) \right\}. \quad (22)$$

6) For surfaces, which are intrinsically 2-dimensional in parametric space, only two of the above sets are to be included for getting the source node.

The geodesic approach discussed above is validated by performing experiments on an aluminum plate and the accuracy of the algorithm in locating the crack position is studied.

d. Experimental details

Experiments were conducted on an aluminum plate of dimensions *400mm x 400mm x 1.6mm*. The PZT sensors *S1, S2, S3, S4* were bonded at locations (x1=0mm, y1=0mm), (x2=0mm, y2=400mm), (x3=400mm, y3=400mm), (x4=400mm, y4=0mm) respectively on the plate. Damage in the form of crack of length 25mm is introduced in the plate as shown in the schematic diagram (Fig. 14). A narrowband Hanning window toneburst signal of five cycles centered at 100KHz was applied to the sensor to generate the A_0 Lamb wave mode in the structure. Huang *et al.* [35] experimentally showed the transduction mechanism affects the axi-symmetric nature of Lamb wave modes excited by the circular PWAS source. However these effects are not

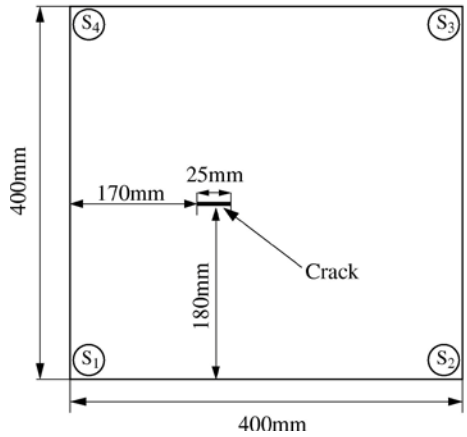

Figure 14. Schematic diagram of the aluminum plate with crack.

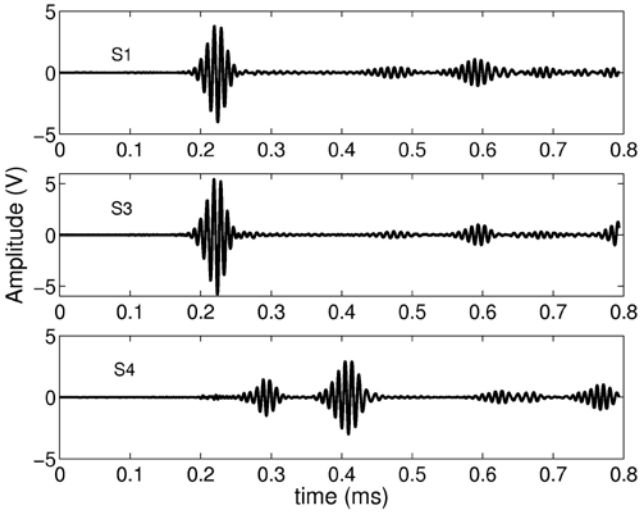

Figure 15. Healthy structure- Signals acquired by the sensors S1, S3, and S4 when sensor S2 is excited.

dominant, if PWAS is excited with frequencies away from their natural frequencies and they can be safely considered as axi-symmetric sources [36]. Furthermore, we assumed that no mode conversion of Lamb wave modes takes place in the structure.

The signals recorded by sensors when sensor *S2* is excited for healthy and damaged structure are shown in Figs. 15, 16 respectively. These signals were analyzed using WT and the wavelet coefficients at 100KHz were computed. The wavelet coefficients of the signals acquired by sensor *S1* for healthy $S_h(t)_{WT}$ and damaged structure $S_d(t)_{WT}$ is shown in Fig. 17. The difference or residual of wavelet coefficients denoted by $S_r(t)_{WT} = S_d(t)_{WT} - S_h(t)_{WT}$ is computed for

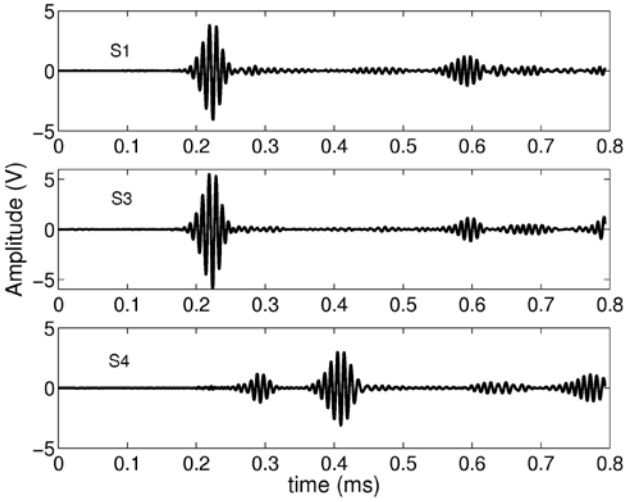

Figure 16. Damaged structure- Signals acquired by the sensors S1, S3, and S4 when sensor S2 is excited.

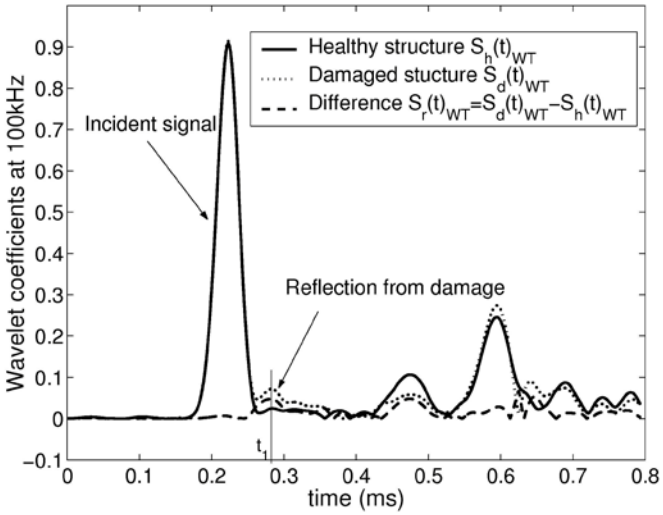

Figure 17. Wavelet coefficients at 100KHz of signals acquired by sensor S1 when sensor S2 is excited under healthy and damage conditions.

sensor *S1*. In $S_r(t)_{WT}$, the direct arrivals of excitation pulses have been removed and it contains only the back-scattered reflection coming from the crack and also from multiple scattering between the crack and the boundaries in the structure (Fig. 17). The arrival time of the reflected waves from damage denoted by t_1 for sensor *S1* is determined using WT and the same procedure is repeated for the other sensors. The arrival-time difference information between the sensors ($dt_{13}, dt_{14}, dt_{34}$) is then used along with the computed discrete geodesics on the mesh using FMM

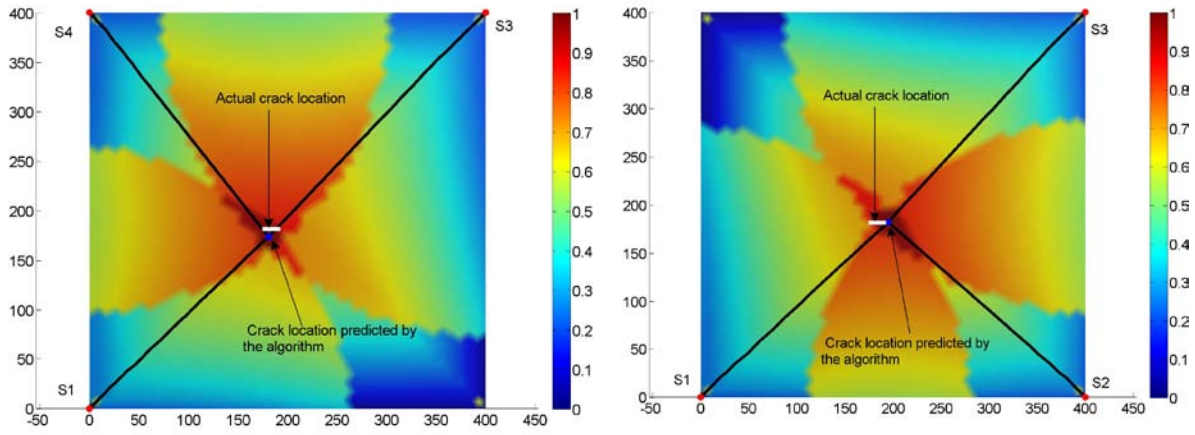

(a) (b)

Figure 18. Aluminum plate with crack: Location of damage computed using the algorithm by excitation of (a) Sensor S2 (b) Sensor S4.

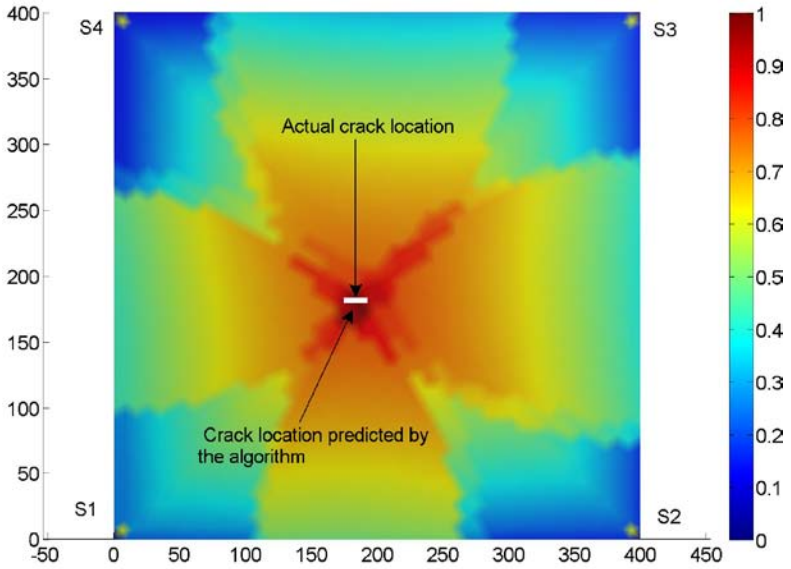

Figure 19. Aluminum plate with crack: Location of damage computed using the all the sensor by geodesic algorithm.

from the sensors to locate the crack. The shortest path taken by the wave from the sensors and their intersection gives the location of the defect as shown in Fig. 18a. The same procedure is repeated for the other sensors and the result for sensor *S4* is shown in Fig. 18b. Finally, all the sensors results were combined together and the location of the defect was estimated quite accurately as shown in Fig. 19. The crack center location computed by the algorithm is given by

(x=185mm, y=176mm) and the result shows a deviation of 3.9 percent from the actual crack center position (x0=182.5mm, y0=180mm).

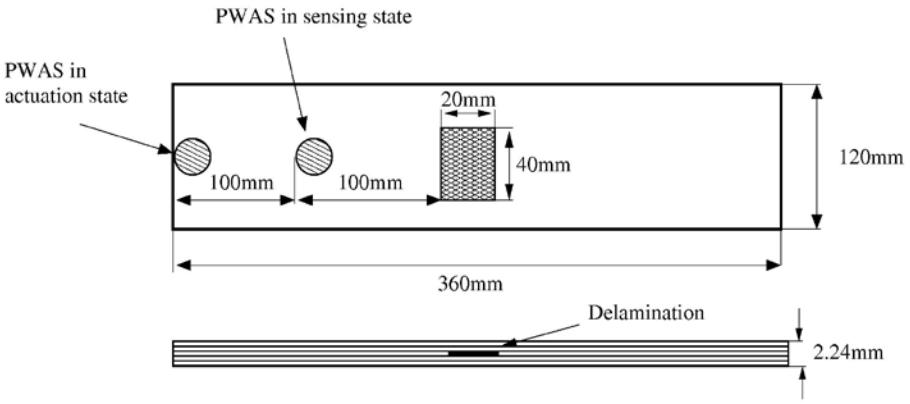

Figure 20. Schematic diagram of the glass-epoxy composite beam with delamination.

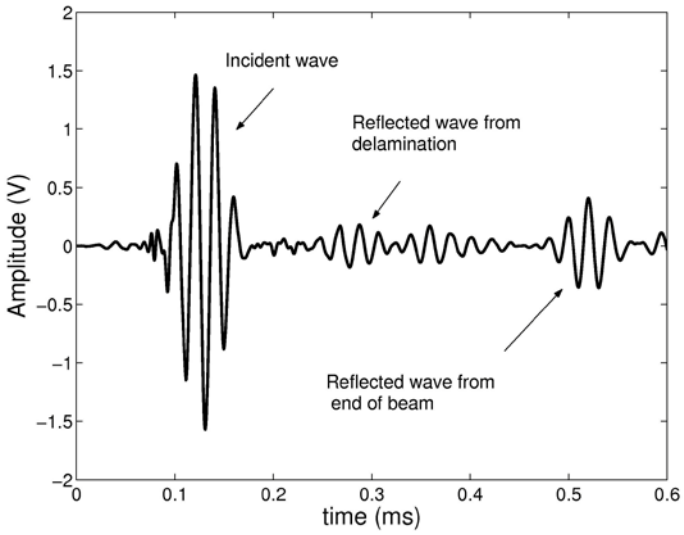

Figure 21. Sensor signal showing the first reflected packet from delamination.

VII. DELAMINATED COMPOSITE BEAM: NUMERICAL AND EXPERIMENTAL STUDIES

The schematic diagram in Fig. 20 shows a unidirectional glass-epoxy composite beam (12 layers) of length 360mm and a cross-sectional area of 2.4mm thickness x 120mm width with an induced delamination which is considered for the experimental study. The delamination dimensions were chosen to be 20mm in length and 40mm in width. The delamination was simulated by inserting a release film between sixth and seventh layer in the beam. The center of delamination is kept at a

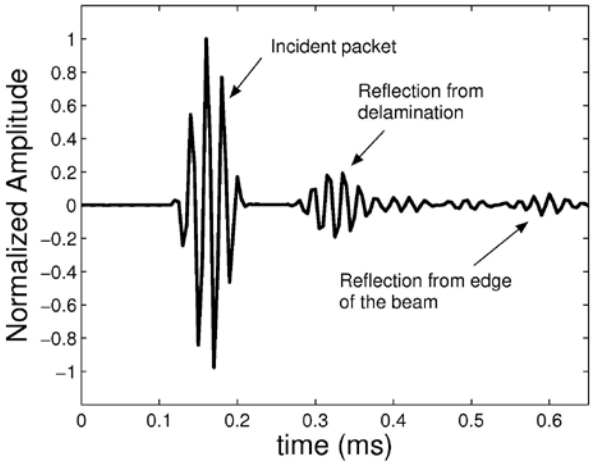

Figure 22. SFEM modeling of composite beam with delamination: Normalized amplitude of transverse velocity at node 2 under narrowband excitation.

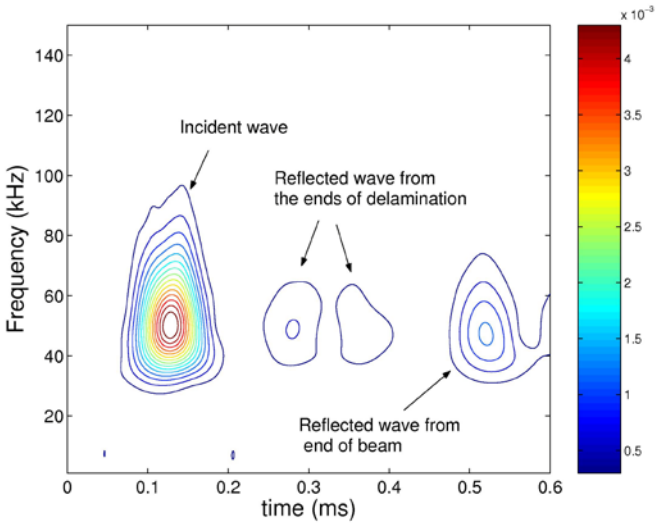

Figure 23. Composite beam with delamination: Continuous wavelet transform of the experimental signal under narrowband excitation.

distance of 210mm from the left end of the beam. The toneburst signal centered at 50KHz was used to excite the PWAS actuator. The sensor was bonded at a distance of 100mm from the PWAS actuator and the signal picked up by the sensor in Fig. 21 shows the reflection of waves from the delamination.

In order to validate the results of the above experiment, numerical simulation was carried out using Spectral finite element method. A unidirectional glass-epoxy composite beam of same dimensions as used in experimental study is considered for the numerical study. For a uni-directional glass/epoxy composite the material properties used for calculations are: E_1=30GPa,

E_2=E_3=10GPa, G_{12}=G_{13}=4.7GPa, G_{23}=3.2GPa, $\gamma_{12} = \gamma_{13} = 0.254$, $\gamma_{23} = 0.428$, $\rho = 2100\text{kg/m}^3$. A single frequency five cycle toneburst sinusoidal pulse modulated at 50KHz is applied transversely at the left end of the beam to generate the first anti-symmetric mode (A_0) in the beam. The delamination in the beam is modeled using four spectral finite elements (Fig. 1). The delamination dimensions were chosen to be 20mm in length and 40mm in width. The transverse velocity is picked up at a distance of 100mm from the left end of the beam and is shown in Fig. 22. Under narrowband excitation, the dispersion of the A_0 mode is minimal and the reflection of waves from the delamination is closer to the experimental results.

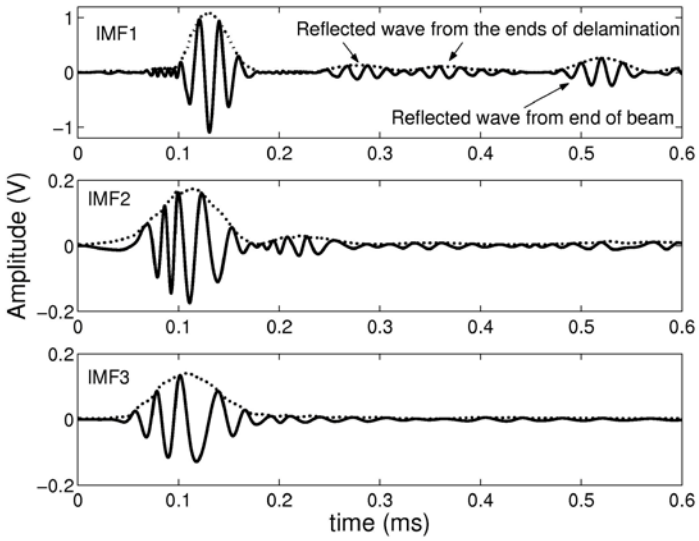

Figure 24. Composite beam with delamination: Empirical mode decomposition of the experimental signal under narrowband excitation.

WT is applied to the signal and the contour plot of the wavelet coefficients is shown in Fig. 23. The contour plot shows the spread of the elastic wave in the time-frequency plane and shows the dispersive nature of the reflected waves from the delamination. The contour plot also shows clearly the reflection of waves from both the ends of the delamination, thereby providing us with the information about its size. HHT is then applied to the signal and the first three intrinsic mode functions (IMF) computed using empirical mode function is shown in Fig. 24. In the first IMF, unwanted oscillations are removed and the envelope of the IMF shows the reflection of waves from delamination and edge of the beam. The amplitude of the second and third IMF is very small and does not provide any useful information about damage in the beam.

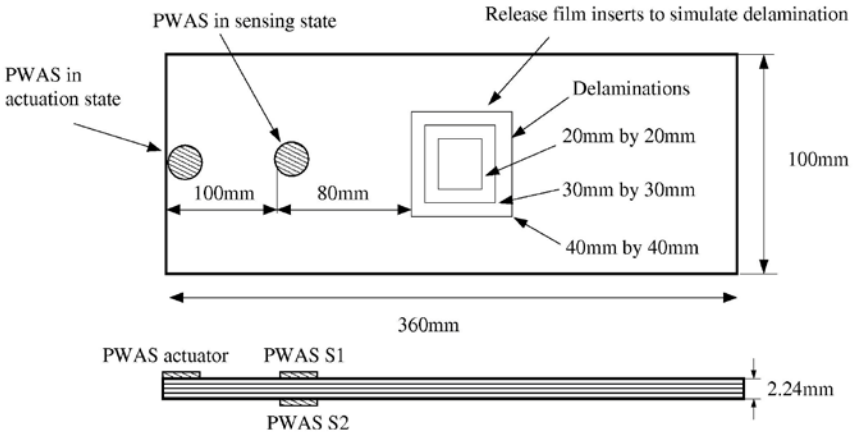

Figure 25. Schematic diagram of the glass-epoxy composite beam with multiple delamination.

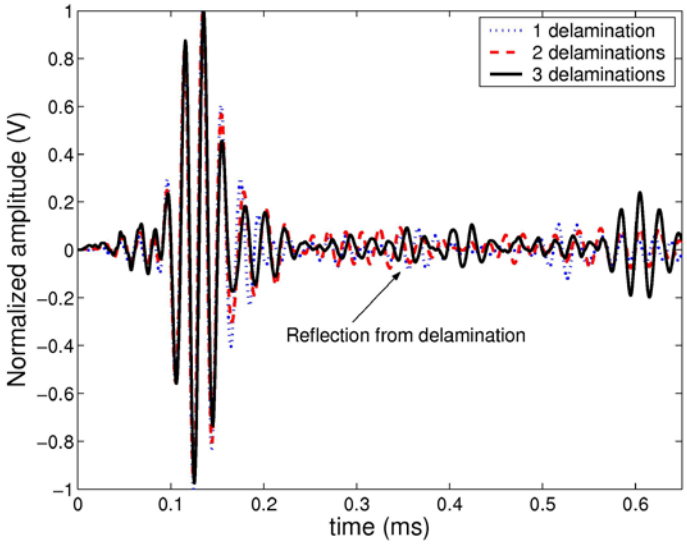

Figure 26. Quasi-isotropic composite beam with delaminations: Time signal picked up by sensor S1 bonded on top surface of the beam.

a. Multi-layer delamination

Further experiments were conducted on a glass-epoxy composite $[0/90/45/-45/0/90]_S$ beams of length 360mm and having a cross-sectional area of 2.4mm thickness x 120mm width. Three different cases of delamination were studied by actuation of the A_0 mode with central frequency of 50KHz in the beam. In the first case, a delamination of size 40mm x 40mm was simulated by inserting the release film between the third and fourth layers from the top surface of the beam. In the second case, two release films of size 40mm x 40mm and 30mm x 30mm were inserted

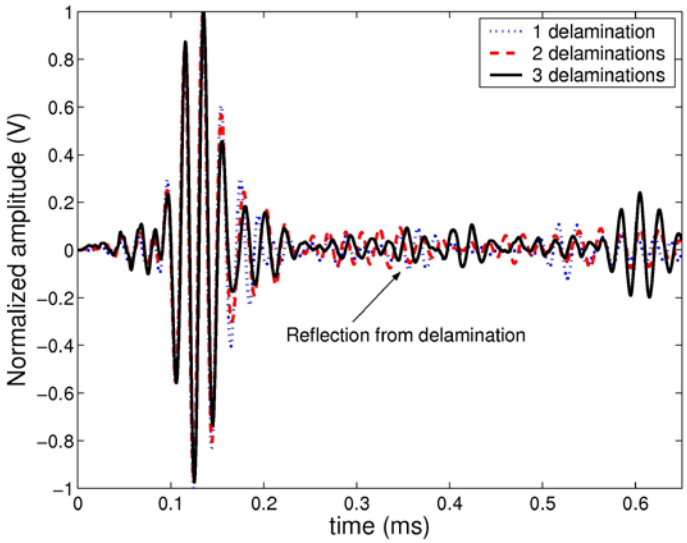

Figure 27. Quasi-isotropic composite beam with delaminations: Time signal picked up by sensor S2 surface bonded on bottom surface of the beam.

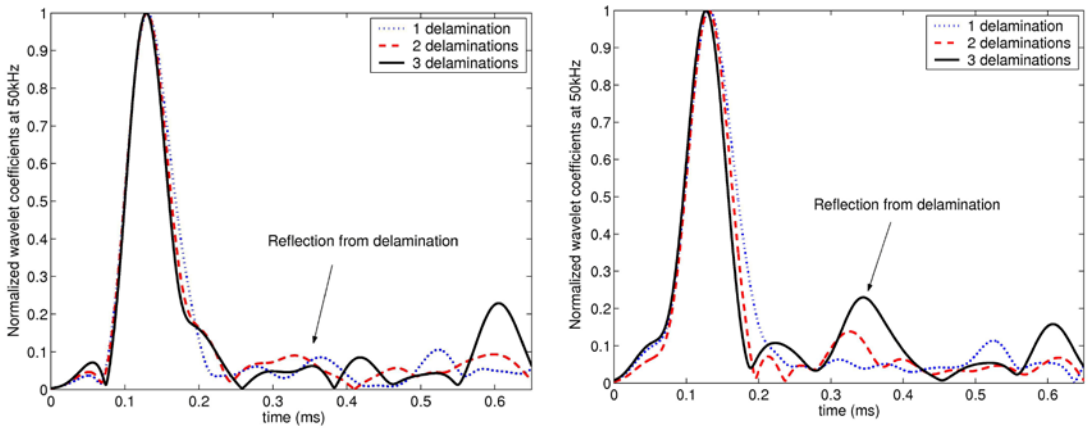

(a) (b)

Figure 28. Wavelet transform coefficients at 50KHz (a) Sensor S1 (b) Sensor S2.

between the third and fourth, fourth and fifth layers of the beam respectively. In the third case, three release films of size 40mm x 40mm, 30mm x 30mm, 20mm x 20mm were inserted between the third and fourth, fourth and fifth, fifth and sixth layers of the composite beam respectively. The schematic diagram of the composite beam is shown in Fig. 25. The sensors *S1* and *S2* were bonded on the top and bottom surfaces of the beam at a distance of 100mm from the actuator, respectively. The sensor *S1* bonded on the top surface was closer to the delamination than sensor

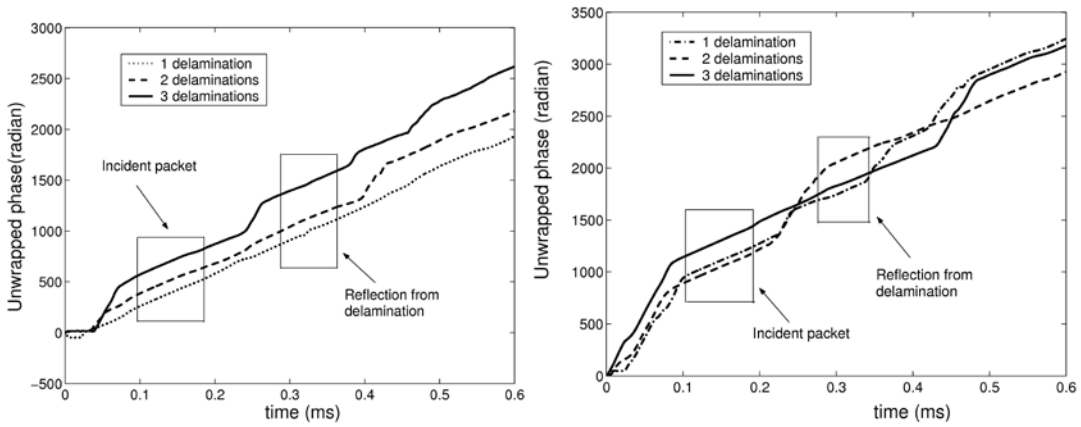

(a) (b)

Figure 29. Unwrapped phase of IMF1 (a) Sensor S1 (b) Sensor S2.

S2. The signals picked up by sensor *S1*, *S2* are shown in Figs. 26, 27 respectively. From the Fig. 26, it can be seen that the amplitude of reflection of waves from the delamination picked up by the sensor *S1* showed less variation. This can be attributed to a weak interaction of the A_0 mode with the delamination. In the case of sensor *S2*, the amplitude of reflection of waves increased with the number of delamination (Fig. 27) and this is due to more interaction of the A_0 mode with the delamination. WT is applied to the sensor signals *S1* and *S2*. The wavelet coefficients at 50KHz is computed and plotted in Fig. 28. The variation of the wavelet coefficients for *S1* with the number of delamination layers was not significant. In the case of *S2*, the variation of the wavelet coefficients increased with the number of delamination layers. HHT is then applied to the signals picked up by *S1*, *S2* and the IMFs of the signals are computed. The unwrapped phase is computed only for IMF1 and the variation of phase with time for sensors *S1*, *S2* is shown in Fig. 29. The local changes of slope of the unwrapped phase of signals indicate the presence of delamination in the beam. The unwrapped phase slope is initially constant across the incident signal, then a jump occurs showing the presence of damage and again the slope is constant across the reflected waves from delaminations. In the case of HHT, the reflection of waves from delamination picked up by sensors *S1*, *S2* is clearly observed in the unwrapped phase plot compared to the WT.

VI. CONCLUSIONS

Lamb wave propagation methods were employed along with time-frequency signal processing techniques for damage detection in metallic as well as composite structure with realistic damage situations. Experiments were conducted on aluminum plates with different crack configurations and the signals analyzed in the time-frequency plane were able to differentiate them. In the case of WT, the wavelet coefficients computed at 200KHz showed that wave scattering is more for 0^o, 45^o crack orientation than 90^o. In the case of HHT, the unwrapped phase of the first intrinsic mode functions also showed that wave scattering is more for 0^o, 45^o crack orientation than 90^o. Further in the experiments conducted on a titanium turbine blade with complex geometry, Lamb waves were able to detect a fine surface crack.

The existing geodesic approach is improved by using FMM to compute accurately the discrete geodesics on the triangular mesh. The relation of geodesics to damage location problem was established by proving that location of damage is the first intersection point of multiple geodesics from the sensors. The approach was experimentally validated in an aluminum plate to identify the crack location.

Experiments were then conducted on glass-epoxy composite beam specimens with delaminations of different sizes and at different locations. SFEM was used to simulate the Lamb wave propagation in composite beam with delamination and the result is in close agreement with the experimental result. Furthermore, the interactions of A0 mode with multiple layer delaminations in composite beams were studied. WT and HHT were used to analyze the experimental signals and were able to identify the damage location and the size of the delamination in the structure. Thus, Lamb waves generated by PWAS with time-frequency analysis technique could be used effectively for damage detection in metallic and composite structures.

REFERENCES

[1] V. Guirguitiu, J. Bao, W. Zhao, “Piezoelectric wafer active sensors embedded ultrasonics in beams and plates”, Experimental mechanics, vol. 43, 2003, pp. 428-449.

[2] V. Guirgiutiu, A. N. Zagrai, “Embedded self-sensing Piezoelectric active sensors for online structural identification”, Journal of Vibration and Acoustics, vol.124, 2002, pp. 117-125.

[3] J. B. Ihn, F. K. Chang, "Detection and monitoring of hidden fatigue crack growth using a built-in piezoelectric sensor/actuator network: I. Diagnostics", Smart materials and structures, vol. 13, 2004, pp. 609-620.

[4] J. B. Ihn, F. K. Chang, "Detection and monitoring of hidden fatigue crack growth using a built-in piezoelectric sensor/actuator network: II. Validation using riveted joints and repair patches", Smart materials and structures, vol. 13, 2004, pp. 621-630.

[5] S. Hurlebaus, L. Gaul, "Smart layer for damage diagnostics", Journal of Intelligent Material Systems and Structures, vol. 15, no. 9-10, 2004, pp. 729-736.

[6] N. Guo, P. Cawley, "The interaction of Lamb waves with delaminations in composite laminates", Journal of Acoustical society of America, vol. 94, no. 4, 1993, pp. 2240-2246.

[7] C.A. Paget, Sebastien Grondel, Klas Levin, Christophe Delabarre, "Damage assessment in composites by Lamb waves and wavelet coefficients", Smart materials and Structures, vol. 12, 2003, pp. 393-402.

[8] Z. Su, L. Ye, Y. Lu, "Guided Lamb waves for identification of damage in composite structures: A Review", Journal of sound and vibration, vol. 295, 2006, pp. 753-780.

[9] J.F. Doyle, "Wave propagation in structures", Springer Verlag, 1997.

[10] D.R. Mahapatra, S. Gopalakrishnan and T.S. Sankar, "Spectral-element-based solution for wave propagation analysis of multiply connected composite beams", Journal of Sound and Vibration, vol. 237, no. 5, 2001, pp. 819-836.

[11] D.R. Mahapatra, S. Gopalakrishnan, T.S. Sankar, "Scattering and transmission of mixed-mode waves in delaminated thick composite beams", Proceedings of 2001 ASME Design Engineering and Technical Conference, September 9-12 2001, Pittsburgh, Pennsylvania, USA, DETC01-VIB-21543.

[12] W.H. Prosser, M.D. Seale, "Time-frequency analysis of the dispersion of Lamb modes", Journal of Acoustical Society of America, vol. 105, no. 5, 1999, pp. 2669-2676.

[13] M. Niethammer, L. J. Jacobs, "Time-frequency representations of Lamb waves", Journal of the Acoustical Society of America, vol. 109 no.5, 2001, pp. 1841-1847.

[14] H. Kuttig, M. Niethammer, S. Hurlebaus, L. J. Jacobs, "Model-based analysis of dispersion curves using chirplets", Journal of the Acoustical Society of America, vol.119, no. 4, 2006, pp. 2122-2130.

[15] J. Grabowska, M. Palacz, M. Krawczuk, "Damage identification by wavelet analysis", Mechanical systems and signal processing, vol. 22, no. 7, 2008, pp. 1623-1635.

[16] R. Benz, M. Niethammer, S. Hurlebaus, L. J. Jacobs, "Localization of notches with Lamb waves", Journal of the Acoustical Society of America, vol. 114, no. 2, 2003, pp. 677-685.

[17] K.H. Ip, P.W. Tse, H.Y. Tam, "Extraction of patch-induced Lamb waves using a wavelet transform", Smart materials and Structures, vol. 13, 2004, pp. 861-872.

[18] D. Pines, L. Salvino, "Structural health monitoring using empirical mode decomposition and the Hilbert phase", Journal of Sound and Vibration, vol. 294, 2006, pp. 97-124.

[19] N.E. Huang, Z. Shen, S.R. Long, M.C. Wu, H.H. Shih, Q. Zheng, N.C. Yen, C.C. Tung, H.H. Liu, "The empirical mode decomposition and the Hilbert spectrum for non-linear and non-stationary time series analysis", Proc Royal Soc LondonSeries A - Math, Phys Eng Sci, vol. 454, 1998, pp. 903-95.

[20] A. Apostoloudia, E. Douka, L.J. Hadjileontiadis, I.T. Rekanos, A. Trochidis, "Time-frequency analysis of transient dispersive waves: A comparative study", Applied Acoustics, vol. 68, 2007, pp. 296-309.

[21] J.L. Rose, " Ultrasonic waves in solid media", Cambridge university press, 1999.

[22] S. Mallat, " A Wavelet tour of signal processing", Academic press, 1999.

[23] I. Daubechies, " Ten lecture on Wavelets", SIAM Publications, 1992.

[24] W.M. Karunasena, A.H. Saha, S.K. Datta, "Plane-strain wave scattering by cracks in laminated composite plates", ASCE Journal of Engineering Mechanics, vol. 117, no. 8, 1991, pp. 1738-1754.

[25] D.R. Mahapatra, S. Gopalakrishnan, "A spectral finite element model for analysis of axial-flexural-shearcoupled wave propagation in laminated composite beams", Composite Structures, vol. 59, no. 1, 2002, pp. 67-88.

[26] S. Gopalakrishnan, A. Chakraborty, D.R. Mahapatra, "Spectral Finite Element Method: Wave Propagation, Diagnostics and Control in Anisotropic and Inhomogeneous Structures", Springer, 2007.

[27] A. Nag, D.R. Mahapatra, S. Gopalakrishnan, T.S. Sankar, "A spectral finite element with embedded delamination for modeling of wave scattering in composite beams", Composite Science and Technology, vol. 63, 2003, pp. 2187-2200.

[28] N. Hu, H.H. Wang, B. Yan, H. Fukunaga, D.R. Mahapatra, S. Gopalakrishnan, "The partition of unity finite element method for elastic wave propagation in Reissner-Mindlin plates", International journal of numerical methods in engineering, vol. 70, 2007, pp. 1451-1479.

[29] A.K. Garg, D.R. Mahapatra, S. Suresh, S. Gopalakrishnan, S.N. Omkar, "Estimation of composite model damage parameters using spectral finite element and neural network" Composite Science and Technology, vol. 64, 2004, pp. 2477-2493.

[30] D.R. Mahapatra, S. Suresh, S.N. Omkar, S. Gopalakrishnan, "Estimation of degraded composite laminate properties using acoustic wave propagation model and a reduction-prediction network", Journal of Engineering Computations, vol. 22, no. 7, 2005, pp. 849-876.

[31] M. Kogl, S. Hurlebaus, L. Gaul, "Finite element simulation of non-destructive damage detection with higher harmonics", NDT and E International, vol. 37, no. 3, 2004, pp. 195-205.

[32] R. Gangadharan, G. Prasanna, M. R. Bhat, C. R. L. Murthy, S. Gopalakrishnan, "Acoustic emission source location and damage detection in metallic structure using graph theory based geodesic approach", Smart materials and structures, vol. 18, 2009.

[33] J. A. Sethian, "Level Set Methods and Fast Marching Methods", Cambridge University Press, Cambridge, USA, 2002.

[34] J Sethian and R Kimmel, "Computing geodesic paths on manifolds", Proc. of Natl. Acad. Science, vol. 95, no. 15, 1998, pp. 8431-8435.

[35] H. Huang, T. Pamphile, M. Derriso, "The effect of actuator bending on Lamb wave displacement fields generated by a piezoelectric patch", Smart materials and structures, vol. 17, 2008.

[36] A. Raghavan, C. E. S. Cesnik, "Finite dimensional piezoelectric modeling for guided wave based structural health monitoring", Smart materials and structures vol. 14, 2005, pp. 1448-61.